AD-A086 109 NAVAL RESEARCH LAB WASHINGTON DC F/G 20/7
AN ION BEAM MILLIPROBE FOR MATERIALS ANALYSIS.(U)
MAR 80 R D WILLIS, A R KNUDSON
UNCLASSIFIED NRL-MR-4187 SBIE-AD-E000 433 NL

1 OF 1
AD
A086109

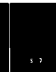
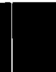

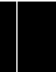

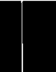

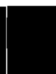

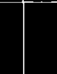

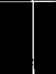
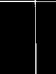

END
DATE
FILMED
8-80
DTIC

ADA086109

SECURITY CLASSIFICATION OF THIS PAGE (When Data Entered)

REPORT DOCUMENTATION PAGE		READ INSTRUCTIONS BEFORE COMPLETING FORM
1. REPORT NUMBER NRL Memorandum Report 4187	2. GOVT ACCESSION NO.	3. RECIPIENT'S CATALOG NUMBER
4. TITLE (and Subtitle) AN ION BEAM MILLIPROBE FOR MATERIALS ANALYSIS		5. TYPE OF REPORT & PERIOD COVERED Final report on an NRL problem
		6. PERFORMING ORG. REPORT NUMBER
7. AUTHOR(s) R. D. Willis and A. R. Knudson		8. CONTRACT OR GRANT NUMBER(s)
9. PERFORMING ORGANIZATION NAME AND ADDRESS Naval Research Laboratory Washington, DC 20375		10. PROGRAM ELEMENT, PROJECT, TASK AREA & WORK UNIT NUMBERS 61153N; RR22-08-44; 0424-0-0
11. CONTROLLING OFFICE NAME AND ADDRESS		12. REPORT DATE March 21, 1980
		13. NUMBER OF PAGES 25
14. MONITORING AGENCY NAME & ADDRESS(if different from Controlling Office)		15. SECURITY CLASS. (of this report) UNCLASSIFIED
		15a. DECLASSIFICATION/DOWNGRADING SCHEDULE

16. DISTRIBUTION STATEMENT (of this Report)

Approved for public release; distribution unlimited.

17. DISTRIBUTION STATEMENT (of the abstract entered in Block 20, if different from Report)

18. SUPPLEMENTARY NOTES

19. KEY WORDS (Continue on reverse side if necessary and identify by block number)

Ion beam analysis
Ion microprobe
Ion implantation
Laser annealing
Materials analysis

20. ABSTRACT (Continue on reverse side if necessary and identify by block number)

An ion beam "milliprobe" has recently been constructed and tested in the Materials Modification and Analysis Branch and is now being applied to the microanalysis of materials. Singly charged ion beams from the NRL 5-MV Van de Graaff accelerator with energies up to 4 MeV can be utilized. A miniature electrostatic lens in line with a pinhole aperture focuses these ion beams to spot sizes as small as approximately 20 micrometers in diameter (0.8 mil, hence the name "milliprobe"). The sample is positioned in the millibeam by means of a motorized X-Y translation stage which allows
(Continues)

DD FORM 1 JAN 73 1473 EDITION OF 1 NOV 65 IS OBSOLETE
S/N 0102-014-6601

SECURITY CLASSIFICATION OF THIS PAGE (When Data Entered)

20. ABSTRACT (Continued)

one to conduct computer-controlled two-dimension scans of the sample with one-micrometer steps. The milliprobe has been used in conjunction with conventional ion beam analysis techniques to characterize the near-surface regions of alloys and semiconductor materials when good lateral resolution is a requirement. The use of the milliprobe is briefly illustrated in two current studies: (1) wear reduction in stainless steels by the implantation of nitrogen and (2) surface composition changes induced by the laser annealing of silicon that has been implanted with nitrogen.

CONTENTS

Page

1. INTRODUCTION 1

2. DESCRIPTION OF THE NRL MILLIPROBE 1

2.1. Ion Beam Production and Collimation 1

2.2. Beam Focusing 3

2.2.1. The Miniature Electrostatic Lens 3

2.2.2. Alignment 5

2.2.3. Beam Profile Measurements 9

2.3 Sample Analysis 9

3. APPLICATIONS TO MATERIALS ANALYSIS 13

3.1. Introduction 13

3.2. Wear Reduction in Stainless Steel Implanted with ^{15}N 15

3.3. Changes Induced in ^{14}N-Implanted Silicon by Laser Annealing 18

4. CONCLUSION 21

REFERENCES 22

DTIC
ELECTE
JUL 2 1980
S D
B

ACCESSION for
NTIS White Section
DDC Buff Section
UNANNOUNCED
JUSTIFICATION
BY
DISTRIBUTION/AVAILABILITY CODES
Dist. AVAIL. and/or SPECIAL
A

AN ION BEAM MILLIPROBE FOR MATERIALS ANALYSIS

1. INTRODUCTION

Energetic ions provide an excellent probe for characterizing the surface layers of materials. Interest in ion beam analysis of materials during the past decade has led to the development or refinement of a number of useful analytical techniques based on the interaction of energetic charged particles with matter. These techniques include Rutherford backscattering analysis, nuclear reaction analysis, and ion-induced x-ray analysis [1,2].

Conventional beam-focusing systems generally are limited to a lateral resolution of approximately 1 mm or greater. The success of ion beam analysis of materials, however, has prompted a number of laboratories in recent years to develop capabilities for focusing energetic ions into beam spots smaller than 50 micrometers [3-11]. In particular, the observation that the bremsstrahlung continuum is about two orders of magnitude less intense for proton-excited x-ray analysis than for electron excitation [3,4] (as in the electron microprobe) and the resulting increase in sensitivity for the detection of trace elements have provided a strong incentive to move in this direction. Good spatial resolution, combined with the sensitivity, specificity, and depth resolution inherent in ion beam analysis techniques results in a powerful analytical tool sometimes called "the MeV ion beam microprobe," but which we prefer to call the "milliprobe" because the ion beam described here has a diameter of approximately one mil.

The intent of this report is to document the construction and implementation of the ion beam milliprobe in the Materials Modification and Analysis Branch at NRL and to provide information for potential users of the milliprobe's capabilities. The original impetus for developing a milliprobe capability came from the materials modification group, which has been investigating the effects of ion implantation on (1) the corrosion and wear of alloys and (2) the optical properties of semiconductor materials. The mechanisms by which ion implantation affects these properties can be better investigated with the aid of an analytical technique which provides chemical composition information with both good lateral resolution and good depth resolution.

Although the focusing of MeV ion beams down to diameters of a few micrometers has been achieved [4,6], such facilities are costly and time consuming to develop, and the operation of such instruments tends to involve time-consuming checks on alignment. Therefore the design used for the NRL milliprobe has been selected as a compromise between ease of construction and convenience of operation on the one hand and beam spot size and lateral resolution on the other hand.

2. DESCRIPTION OF THE NRL MILLIPROBE

2.1. Ion Beam Production and Collimation

A schematic diagram of the NRL milliprobe beam line is shown in Figure 1. Beams of singly charged particles from the NRL 5-MV Van de Graaff accelerator with energies less than 4 MeV can be used. The ion source may be either a radio-frequency type for gaseous materials or a Hill-Nelson type for solid (e.g., metallic) materials. The output of the accelerator is collimated by two rectangular slits prior to a switching magnet, which

Note: Manuscript submitted January 15, 1980.

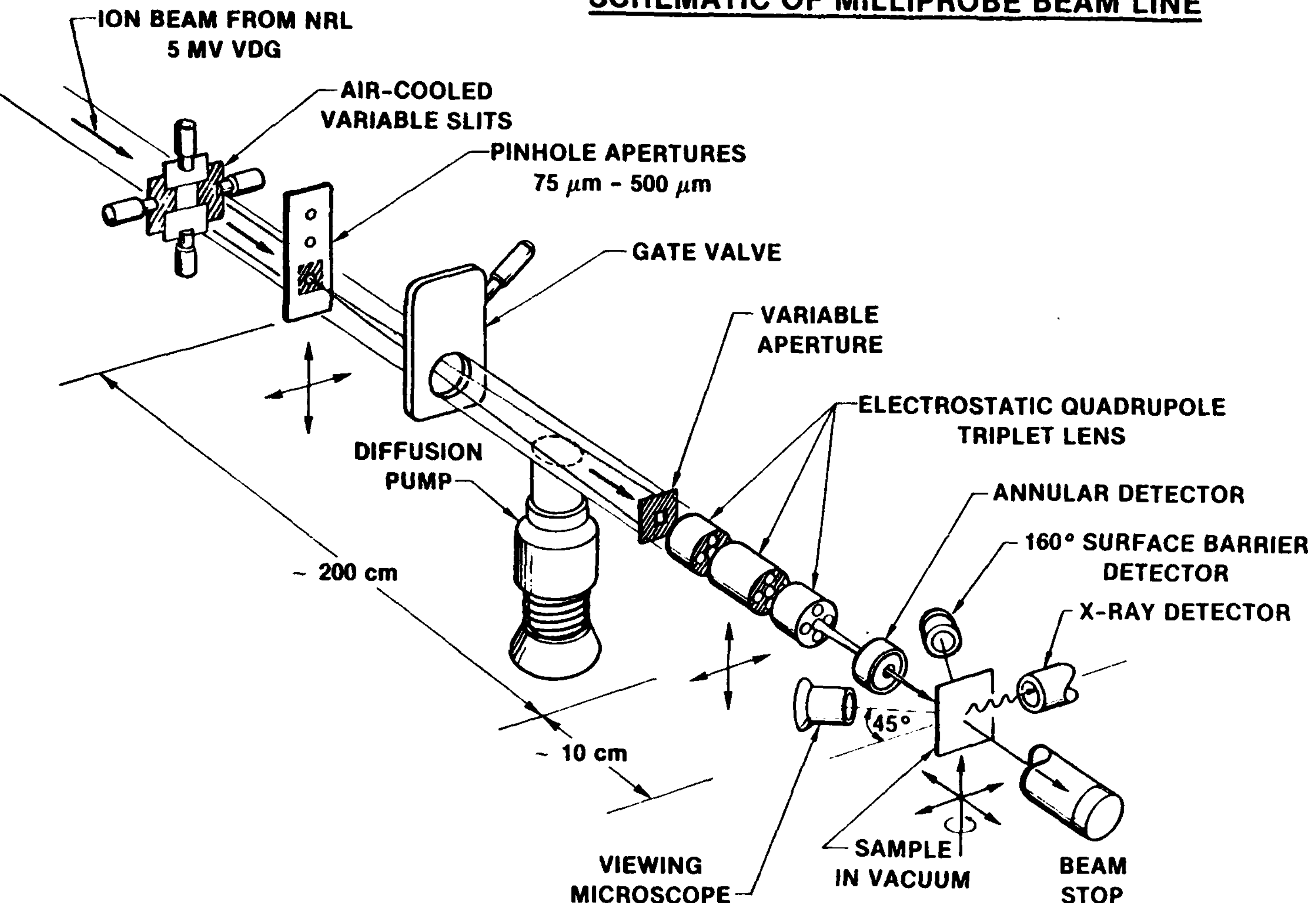

Fig. 1 - Schematic diagram of the NRL milliprobe beam line

directs the beam to the appropriate beam line. Immediately following the switching magnet the beam is further collimated by a third slit, the jaws of which also provide a feedback signal to the energy-stabilizing circuit of the Van de Graaff. A current of 400 nA is typical of the intensity of the transmitted beam, when the post-magnet slit has an opening 300 μm x 300 μm.

Approximately ten centimeters downstream from the post-magnet slit is the pinhole aperture box. This unit houses a vertical ladder which can be positioned precisely in the X (horizontal) and Y (vertical) directions by means of micrometer positioning devices. Pinholes ranging from 75 μm to 400 μm in diameter have been drilled (with a precision drill press) into strips of 3-mil tantalum, which can be mounted onto the pinhole ladder. These pinholes serve as the object for the beam-focusing lens located approximately two meters downstream. A quartz piece attached to the pinhole ladder fluoresces under bombardment by the beam, thus providing an image of the beam as an aid to pinhole alignment. The pinhole ladder can be fully retracted from the beam path to make the beam line usable for other experiments.

Final collimation of the ion beam is achieved by a rectangular aperture attached to the upstream end of the focusing lens (Figure 2). The opening of this aperture can be varied from 0.5 mm on a side to 1.5 mm on a side. However, optimal performance of the focusing lens is obtained with the smallest lens aperture. The purpose of the lens aperture is twofold: (1) by limiting the transmitted beam to the central region of the lens bore, the aperture minimizes aberration effects and (2) the aperture provides information on the beam position which is critical to proper alignment of the system (Section 2.2.2).

In a typical experiment in which a 250-μm pinhole is used as the object, the four tantalum sector plates (Figure 2) will intercept approximately 40 nA of beam current, allowing 2-3 nA of beam to pass through the aperture and be focused onto the sample.

2.2. Beam Focusing

2.2.1. The Miniature Electrostatic Lens

Focusing of the ion beam is accomplished by an electrostatic quadrupole triplet constructed at NRL and modelled after a design by Augustyniak et al. [5]. Cross-section views of the lens in two vertical planes are shown schematically in Figure 2. The lens is 11 cm long and 1.9 cm in diameter, with a bore diameter of 2 mm through which the ion beam passes. As used in the present arrangement, the lens has a focal length of approximately 10 cm.

The lens electrodes are formed on a set of four metallized sapphire rods (centerless ground and polished to a fine diamond finish) which are set into precisely aligned holes bored into Vespel [12] insulating pieces. Metallization of the rods was achieved by evaporation of niobium with the rods held in a rotating jig. Insulating gaps, 3 mm wide and located 30 mm from the ends of each rod, were created by masking off these areas during the evaporations. Each rod thus forms three electrodes with the dimensions shown in Figure 2. The sapphire rods and surrounding insulating blocks are enclosed within a stainless steel housing.

Electrical contact to the twelve electrodes is provided by fine stainless steel springs held captive in hollow screws (Figure 2). In practice, there has been a recurring problem with loss of contact between the springs and the niobium coating. The cause of this contact failure has not been determined, but evidence suggests the formation of a thin oxide layer between the spring and the niobium.

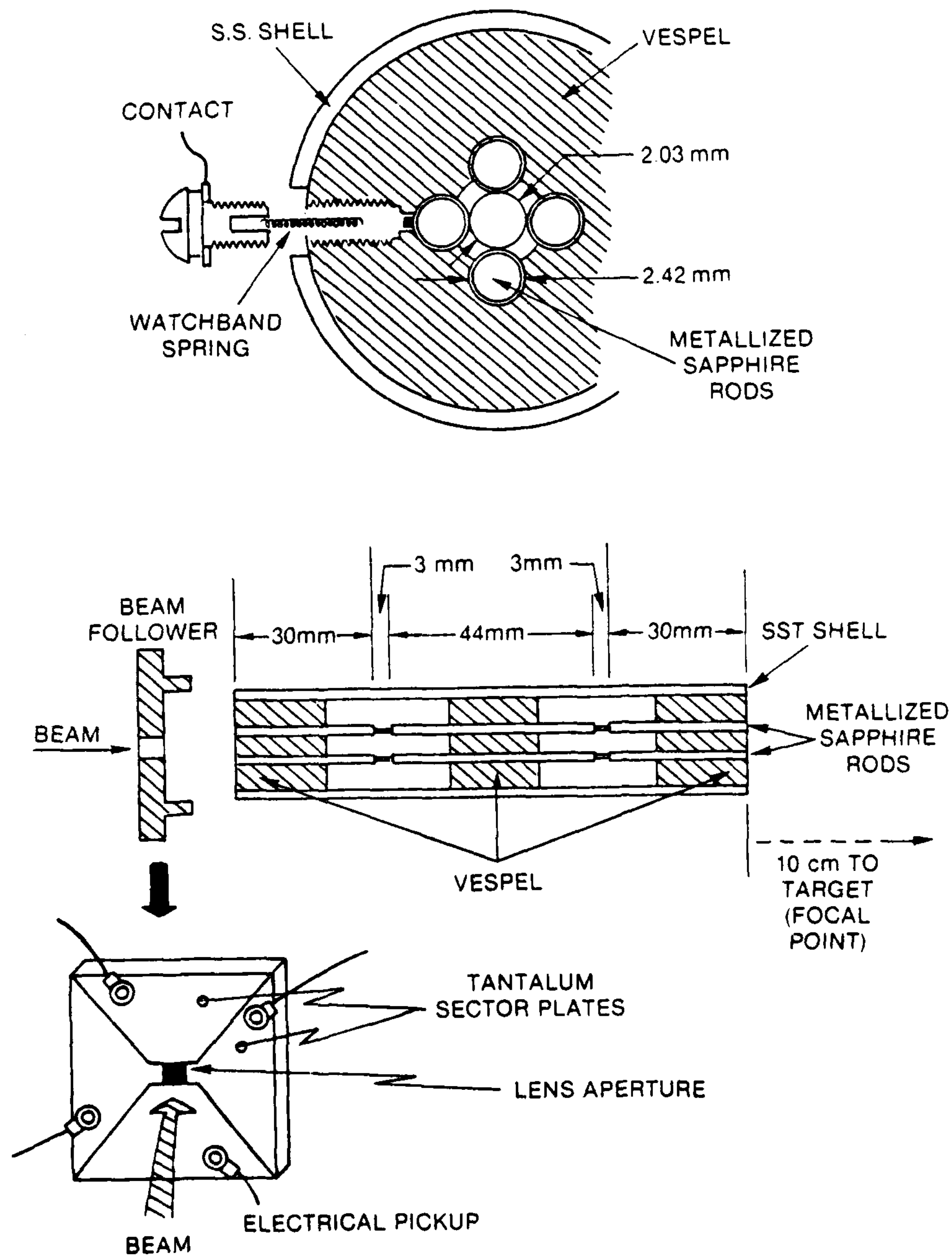

Fig. 2 - Schematic drawings of the miniature electrostatic lens. (Modified from (5).)

Figure 3 is a sketch of the electrical connections to the lens. The lens is operated as a symmetric triplet, the two end elements being identically excited. The middle element is independently excited and is excited in the opposite sense. The electrical circuit which provides voltage to the lens is shown in Figure 4. Positive and negative voltages are provided by two separate power supplies. Voltage to the end-poles and mid-poles are independently adjusted by means of two ten-turn dials, each coupled to a pair of 300-kΩ potentiometers. By adjusting one or both of the dials, one can vary the voltage applied to the corresponding electrodes continuously over the range from 50% to 95% of the voltage selected on the power supply. All voltages from 0.3 kV to 2.85 kV are accessible; however the power rating of the resistor string shown in Figure 4 limits the maximum voltage to 2700 V. Operating between 0 V and 2700 V, the lens is capable of focusing singly charged ions up to approximately 4.2 MeV in energy.

One advantage of the electrostatic lens is that its focusing properties are mass and charge independent. For a given voltage on the terminal of the Van de Graaff beams of H^+, D^+, He^+, and heavier ions will all be focused with the same excitation voltage if no charge exchange occurs between acceleration and focusing. By appropriate adjustment of the end-quad-to-mid-quad voltage ratio, the lens is capable of forming line images (either horizontal or vertical) or rectangular images.

The lens is suspended inside a four-inch Dependex [13] vacuum multicross by means of two supporting/positioning rods. Figure 5 shows the milliprobe lens assembly after removal from the Dependex housing. Each support rod attaches to the lens by means of a copper-beryllium leaf spring which provides flexibility for positioning the lens. The rods extend through vacuum-seal flexible bellows and are rigidly attached to two-axis translation stages. This arrangement facilitates precise alignment of the lens along the beam axis. As with the pinhole ladder, the lens can be fully retracted from the beam path without breaking vacuum in order to clear the beam line for use by other experimenters.

2.2.2. Alignment

Careful alignment of the milliprobe system is a precondition for good focusing action. There are no beam-steering elements on the milliprobe beamline; instead, alignment is achieved by positioning the pinhole aperture, the lens, and the sample to be analyzed on the beam axis. The alignment has been found to be stable (i.e., requiring no repositioning of any components) over an eight-hour period of continuous running.

The pinhole is aligned by adjusting its position until a maximum in the transmitted beam intensity is observed on a quartz viewer located downstream of the pinhole.

The lens aperture is aligned on the beam axis by positioning the upstream end of the lens until the current registered on the beam follower (Figure 2) is balanced—i.e., until the currents incident on opposing sector plates are equal. With no voltage applied to the lens, the downstream end is positioned (by a second X-Y translation stage) until a rectangular image of the lens aperture is observed on a quartz viewer attached to the target ladder. (The target ladder is viewed through a microscope which protrudes into a recessed port on the target chamber at forty-five degrees to the incident beam (Figure 1).) Since adjustment of the position of the downstream end of the lens somewhat affects the upstream end, and vice versa, it is necessary to use several iterations to align the lens. If the lens is properly aligned, the image will focus, without being steered, to a point or line image as lens voltage is applied.

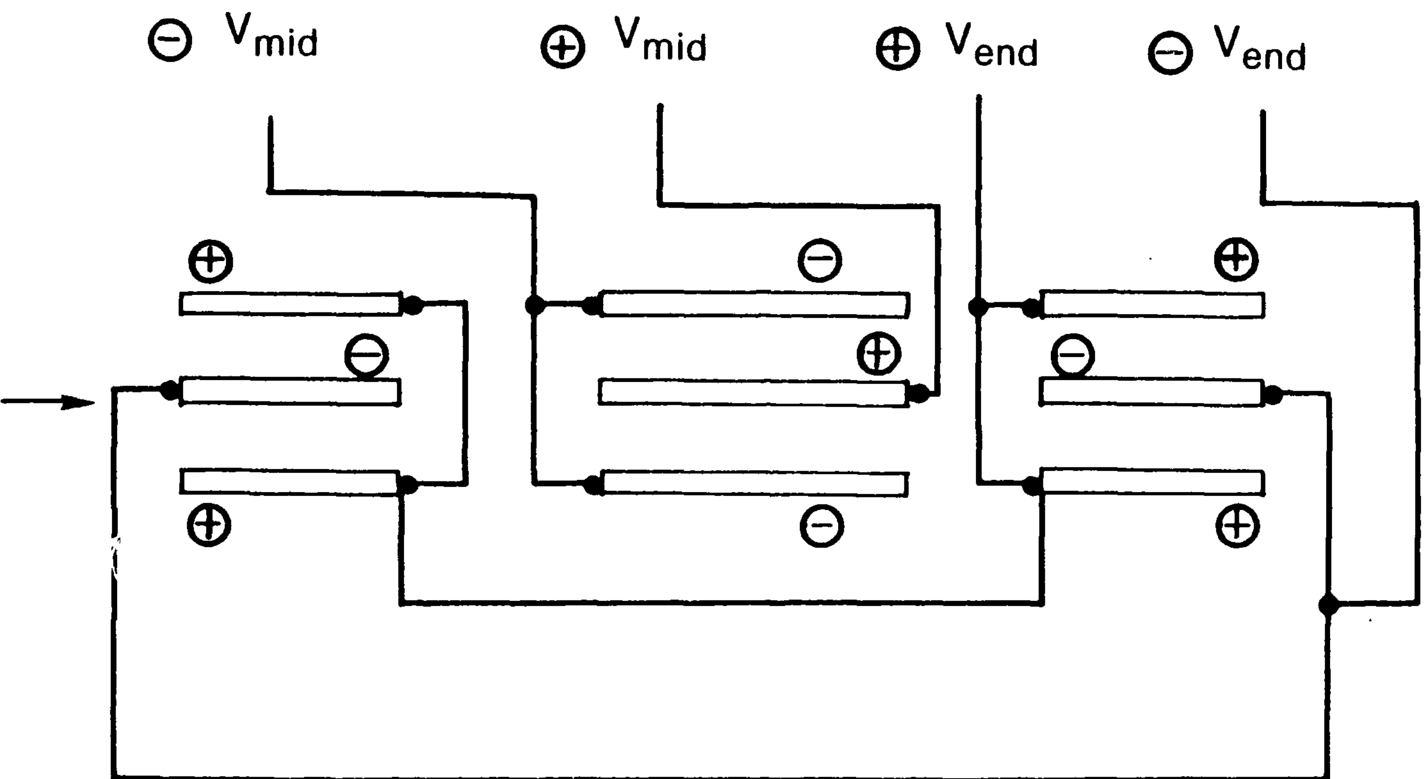

Fig. 3 - Wiring diagram of the lens elements (Modified from (5).)

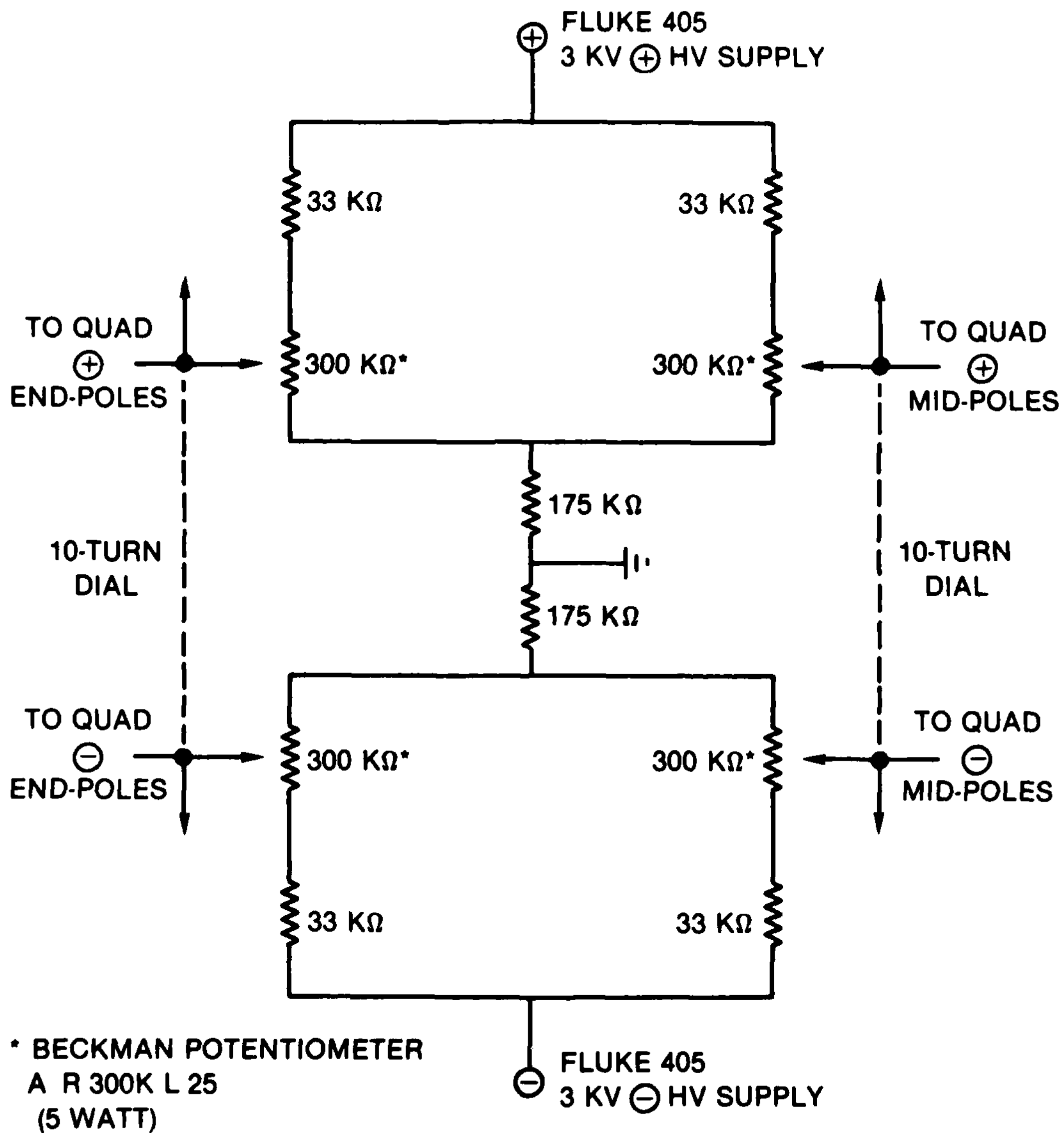

Fig. 4 - Diagram of the electrical circuit used to power the lens

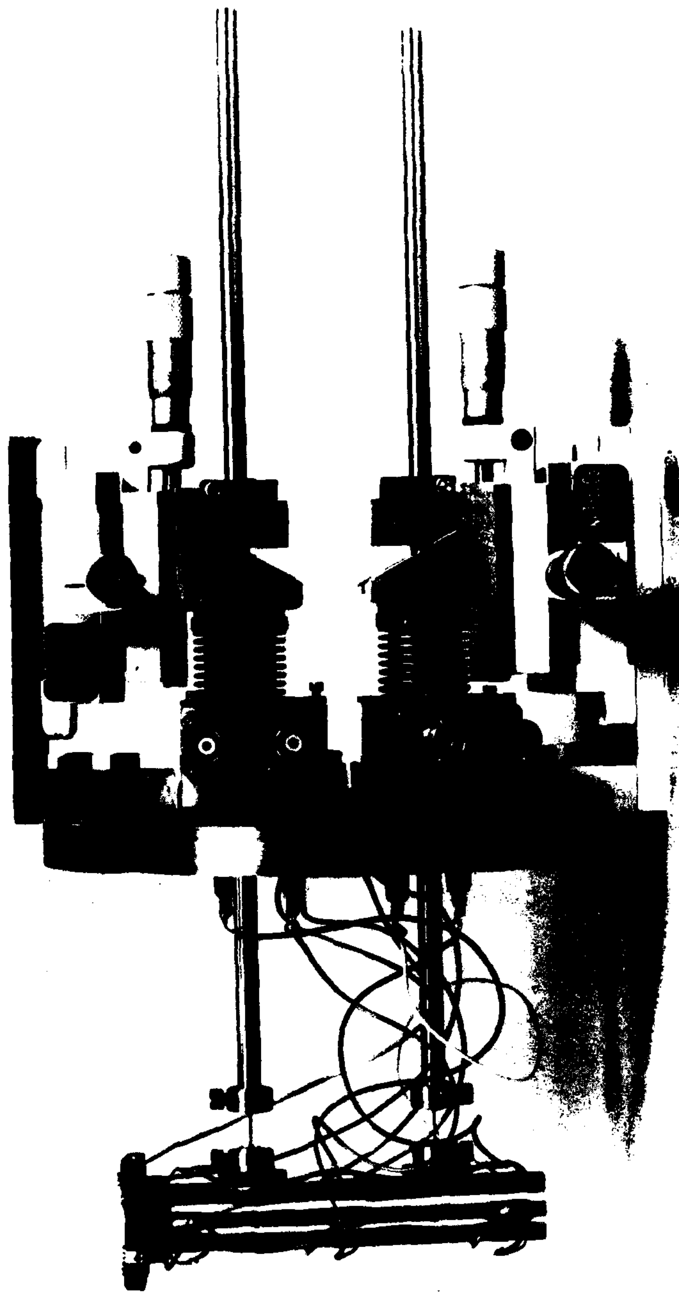

Fig. 5 - Photograph of the milliprobe lens assembly before installation in the beam line.

Samples analyzed with the milliprobe are mounted in vacuum on a target ladder which can be rotated 360 degrees about the vertical axis, and translated in the X, Y, and Z directions by means of precision translation stages. Before positioning the sample in the beam, the location of the beam spot on the target ladder quartz is referenced to a calibration scale internal to the viewing microscope. Next the region of interest on the sample is brought to a focus at the reference location in the microscope field of view by adjustment of the X, Y, and Z translation stages. The sample is then ready to be analyzed.

2.2.3. Beam Profile Measurements

Figure 6 shows several measurements of the beam profile made with pinhole apertures of varying diameter. The lens aperture for these measurements was 0.5 mm on a side. The data were obtained by stepping a two-micrometer-wide gold line, etched on a silicon wafer, across a fixed beam of 2-MeV He^+ while recording the backscattering yield from the gold. A step size of 3 μm was provided by a precision, motor-driven translation stage coupled to the target ladder (Section 2.3.).

Measurements of the width (FWHM) of the beam profiles shows the demagnification of the lens to be approximately 12 for both the 330-μm and 254-μm pinholes. The lesser demagnification (approximately 8) for the 152-μm pinhole is suggestive of limiting aberrations. The current intensity on the target was 1-2 nA for the larger pinholes, and approximately 0.5 nA for the small pinhole.

2.3. Sample Analysis

Analyses of specimens are performed in vacuum in the target chamber shown schematically in Figure 7. Figure 8 shows a portion of the milliprobe beam line, including the lens assembly and the target chamber. The target chamber is comprised of a main chamber (Dependex Multicross) and a vacuum lock separated by a gate valve. The target ladder attaches to an insulated shaft which extends through a vacuum-seal flexible bellows. The bellows is mounted to a three-axis translation stage, which permits movement of the target rod in the X, Y, and Z directions. In addition, the entire lid on the vacuum lock rotates through 360 degrees so that the sample can be oriented at any desired angle to the incident beam. For purposes of changing samples, the target rod can be decoupled from the translation stage and raised into the vacuum lock.

The three-axis translation stage for the target rod was purchased commercially (Ardel Kinematic Corp.). The X (horizontal) and Y (vertical) movements employ stepping motors with a one-micrometer step size which have been interfaced to an on-line computer. Thus one can obtain two-dimension scans of a sample, under computer control, with step sizes as small as one micrometer. The Z positioner (providing motion along the beam axis) is manually operated and is used to position samples of varying thickness at the focal point of the lens. The dimensions of the flexible bellows limit the range of travel of the target to approximately 1.27 cm in any direction.

An area approximately 1.8 by 6.7 cm is available for mounting samples on the surface of the ladder. A sample thickness of a few millimeters or less is convenient, but arrangements can frequently be made to accommodate thicker samples and those of greater lateral extent than that specified above.

Although the power dissipated in the sample by the incident beam is only a few milliwatts, the power density may approach a kilowatt per cm^2 or 10 megawatts per cm^3. Although it has been our experience that no visible damage is produced in metal samples

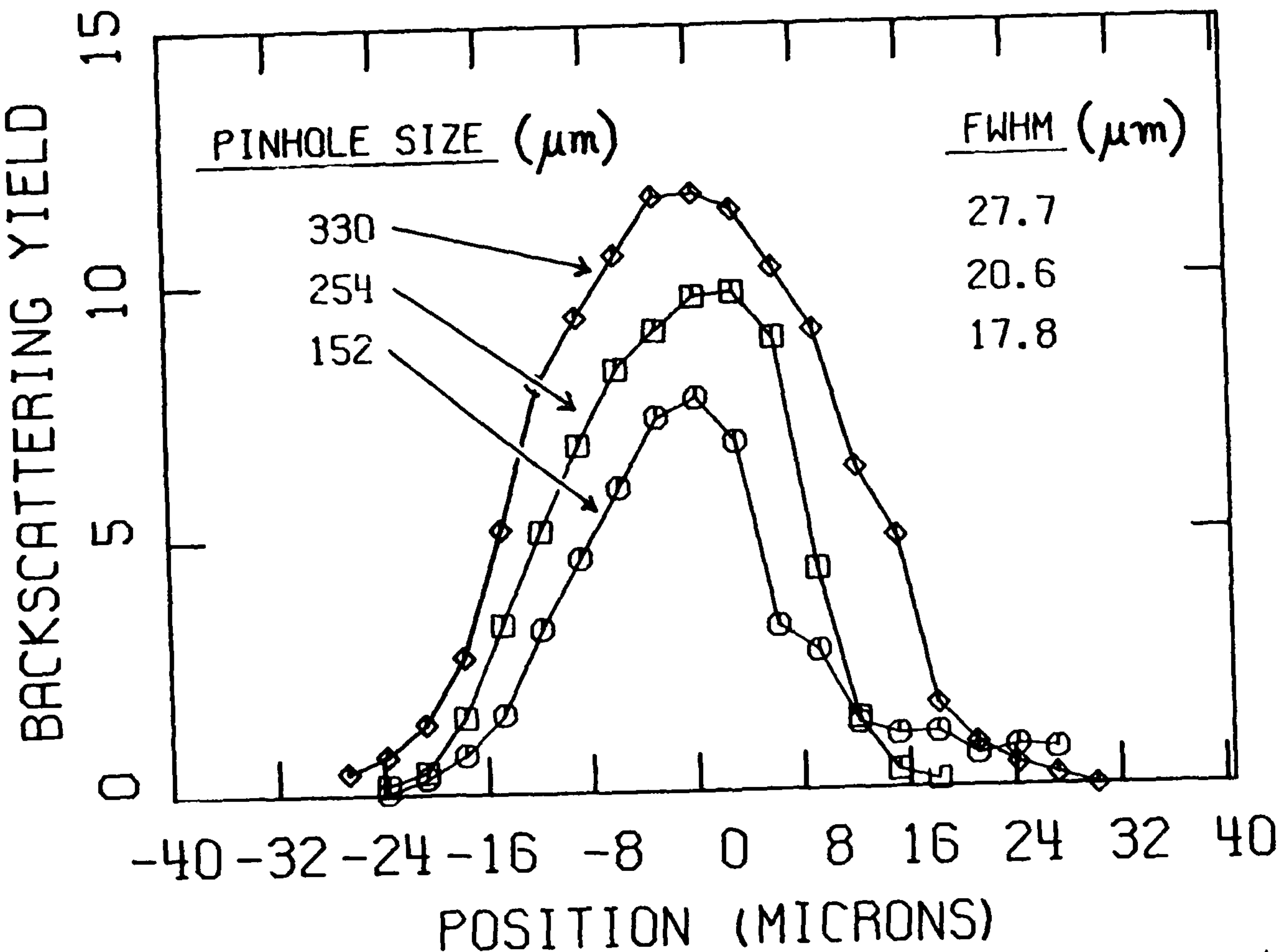

Fig. 6 - Beam profile measurements showing beam diameter versus pinhole size for 2-MeV He^{+} ions. These measurements were made by stepping a two-micrometer gold line, etched on a silicon wafer, across the He beam. The yield of particles scattered from the gold is plotted on the ordinate.

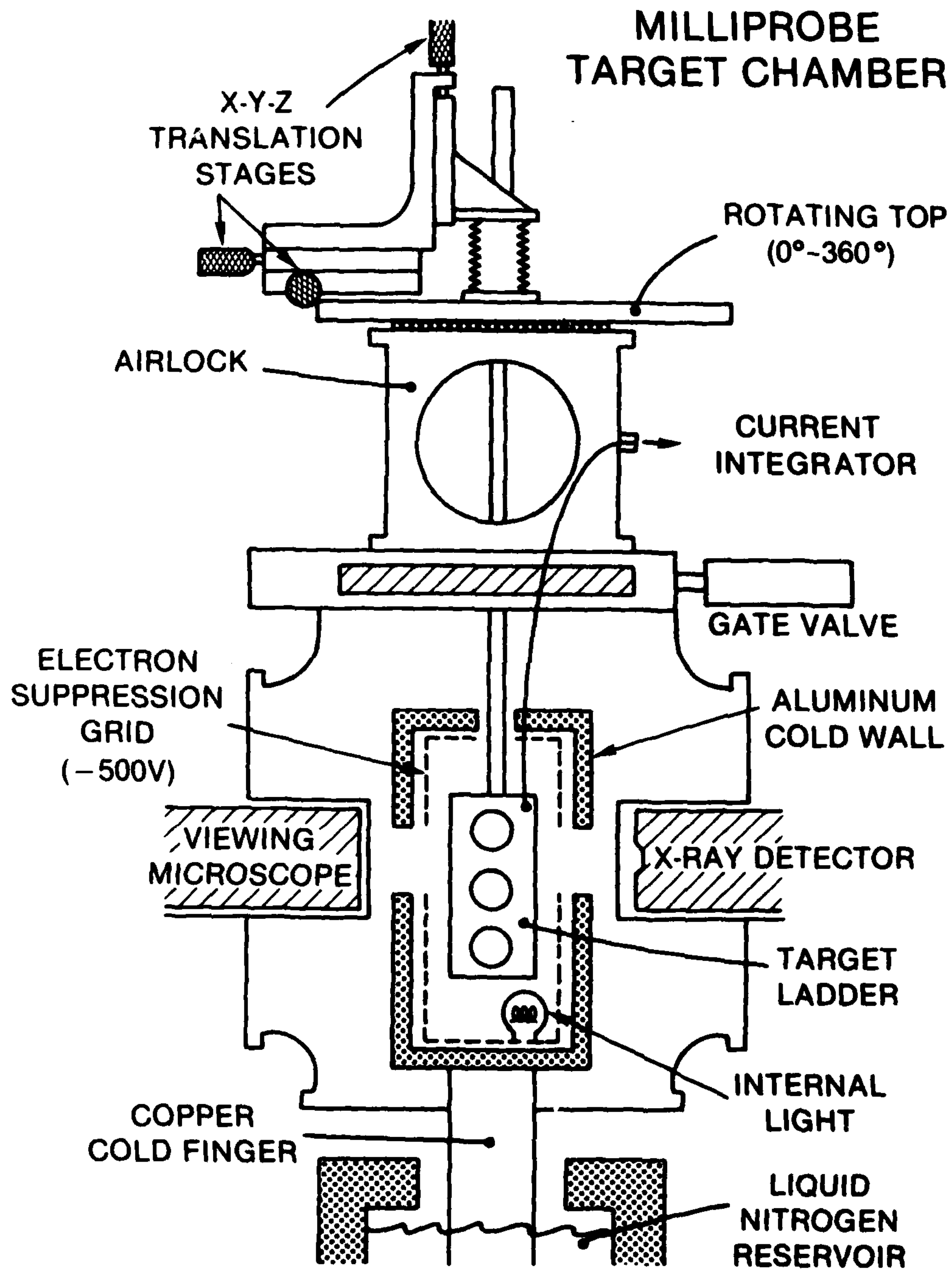

Fig. 7 - Schematic drawing of the milliprobe target chamber

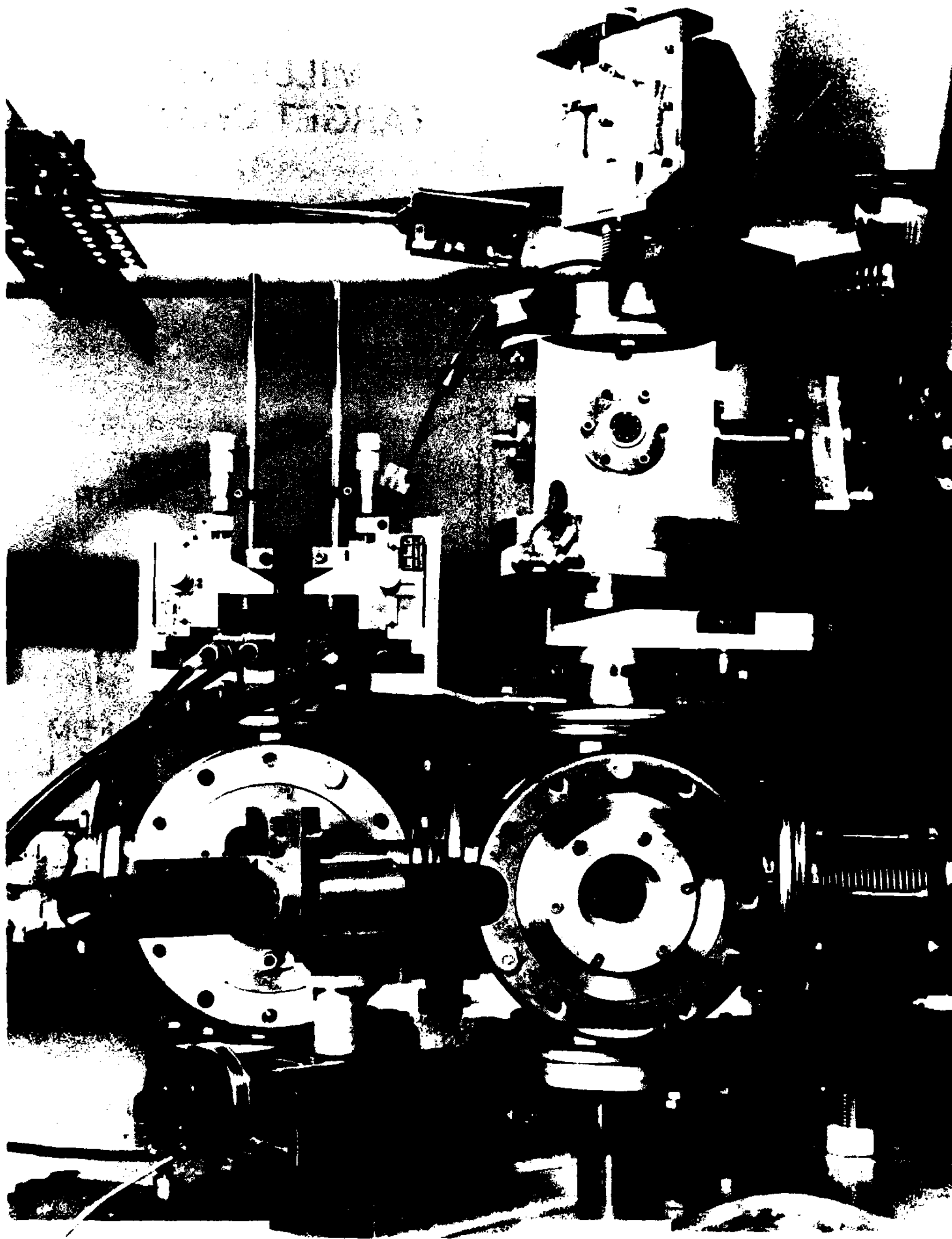

Fig. 8 - Photograph of a portion of the milliprobe beam line including the lens housing (left-hand chamber), viewing microscope, and target chamber (right-hand chamber).

at this power density, the local heating may in some circumstances produce undesirable diffusion. In the case of silicon, visible damage has been produced, but such damage can be avoided by changing from a point focus to a line focus. In some situations such a change may not be feasible, but lower beam currents and longer analysis times may be a possible alternative.

The target ladder is surrounded by a copper mesh grid with a negative bias of 500 V to provide secondary electron suppression. The charge impinging on the sample during analysis is collected directly from the target ladder. Concentric with the suppression grid is a cylindrical aluminum cold wall capped with copper end pieces. A 2.54-cm diameter solid copper rod threads into the bottom of the cold cylinder and extends through a vacuum flange into a liquid nitrogen reservoir. The purpose of the cold cylinder is to trap residual hydrocarbon vapors before they deposit onto the sample during an analysis.

The target chamber is equipped with a custom-built viewing microscope, which views the sample at an angle of 45 degrees to the incident beam direction. The microscope features a magnification of approximately 40 at a working distance of 5.2 cm. Illumination of the target surface is provided by two 6V lamps mounted inside the target chamber.

The target chamber is provided with detectors for both x-rays and charged particles. A recessed port at 90 degrees to the incident beam accommodates a solid-state energy-dispersive x-ray detector. Two surface-barrier detectors (one positioned at 160 degrees and the other, an annular detector, on the beam axis) are available for charged-particle detection. Depending on the particular application, one or more of the following ion beam analysis techniques may be utilized: ion-induced x-ray analysis, nuclear reaction analysis, or Rutherford backscattering analysis. Some examples illustrating the application of the milliprobe to materials analysis are presented in Section 3.

A major difficulty encountered during the development of the milliprobe was the elimination of mechanical vibration in the milliprobe beam line. Several modifications that were made to the system have been effective in reducing the vibration to a tolerable level. The most important change was to mount the lens assembly and target chamber on a massive concrete pillar, thus decoupling them from the adjoining beam line. Then the vibrations arising from a mechanical vacuum pump were minimized by clamping the vacuum hose (which was connected to the diffusion pump) in a heavy vise. The present arrangement of the milliprobe beamline is shown in the photograph of Figure 9.

3. APPLICATIONS TO MATERIALS ANALYSIS

3.1. Introduction

In this concluding section we discuss two recent experiments in the Materials Modification and Analysis Branch to illustrate the application of the ion beam milliprobe to materials analysis. Because the Branch has a major interest in the modification of material properties via ion implantation, much of the work with the milliprobe has been done on ion implanted samples, in conjunction with the materials modification group. The examples which follow are in the nature of exploratory studies intended to illustrate the kinds of information which can be obtained with the milliprobe.

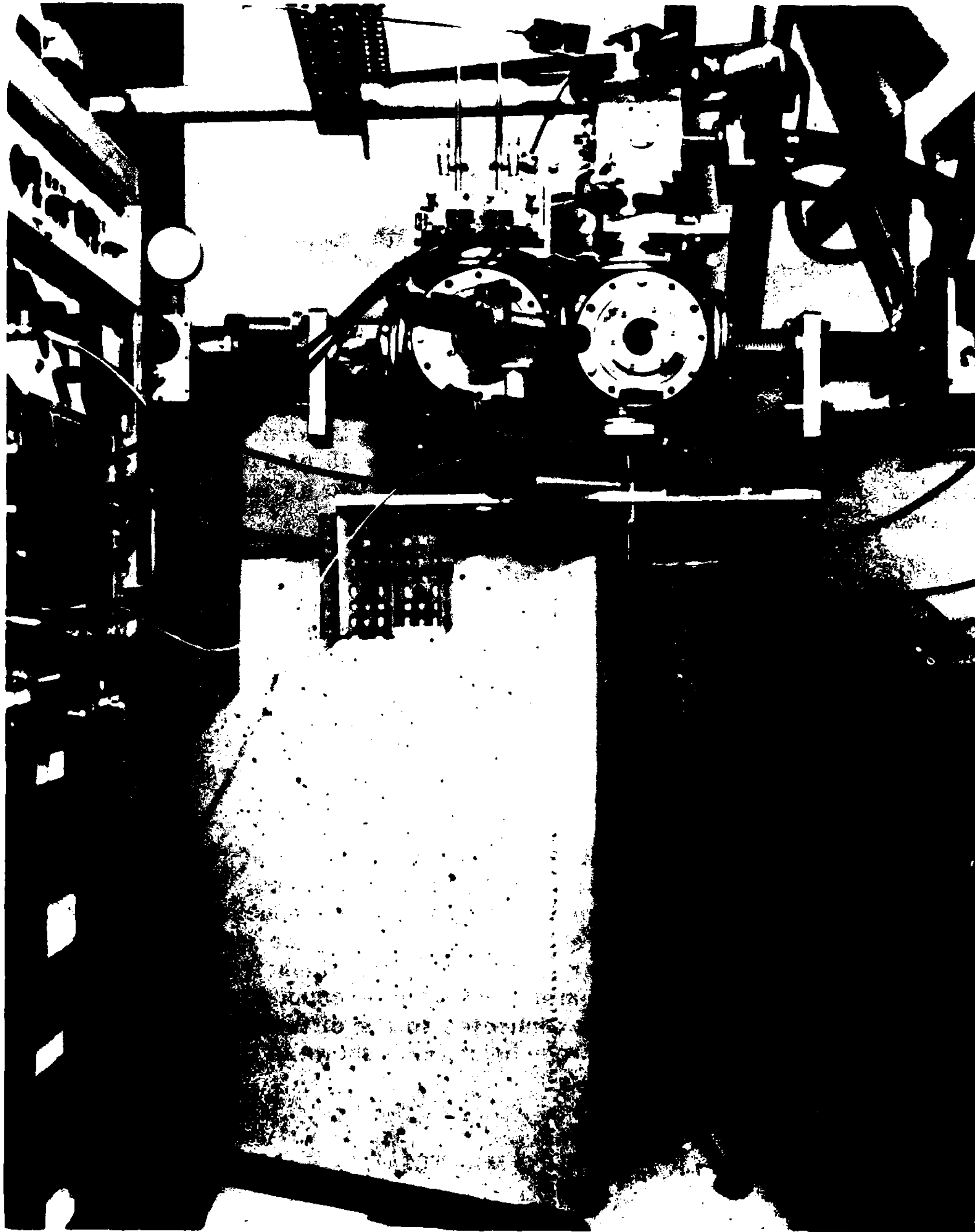

Fig. 9 - Photograph of the milliprobe beam line, showing the electronics rack and the isolated concrete support for the milliprobe components.

3.2. Wear Reduction in ^{15}N Implanted Stainless Steel

Ion implantation is being investigated in the Materials Modification and Analysis Branch as a technique for improving the resistance of metals to wear and fatigue. Wear tests conducted by the Ion Implantation Section show that implantation of nitrogen ions into type-304 stainless steel reduces the sliding wear rate of the material by factors of 25 to 50 [14]. (The wear tests consist of rotating a cylinder of type-304 stainless steel, unimplanted or implanted, against an upper stationary cylinder of unimplanted type-304 stainless steel in a crossed cylinder-on-cylinder geometry, while the upper cylinder is under a dead-weight load.)

The reduction in wear rate is observed to persist even after the implanted sample has been worn far beyond the original depth of the implanted ions. This observation suggests that the implanted ions diffuse under the local heating and stresses occurring during the wear process, perhaps resulting in a continously renewed, wear-resistant surface layer.

The milliprobe was applied to test this hypothesis by measuring the concentration and depth distribution of the implanted nitrogen ions both in and adjacent to the wear scar (typically less than 2 mm wide) for varying amounts of wear. The isotope ^{15}N was chosen for the implanted species because (i) the large cross section and high Q value of the $^{15}N(p,\alpha)^{12}C$ reaction make it a very sensitive, convenient, and definitive tool for detecting and measuring the locations of the nitrogen and (ii) the paucity of the ^{15}N isotope in nature provides the means of distinguishing implanted nitrogen atoms from absorbed atmosphere nitrogen and also from nitrogen remaining in the alloy from the manufacturing process.

Figure 10 shows a representative spectrum obtained with a focused beam (25 μm diameter) of 1.05-MeV H^+ incident on the worn region of an implanted sample. An annular surface-barrier detector was used to detect the outgoing alpha particles in addition to the large flux of backscattered protons. Information about the concentration and depth distribution of the implanted ^{15}N ions in the region exposed to the beam is obtained from the intensity and energy distribution of the alpha-particle spectrum.

The lower half of Figure 11 plots the ^{15}N yield versus position in a transverse scan across part of a wear scar. The 400-μm scan was made by stepping the wear scar across the focused beam and collecting a spectrum similar to Figure 10 at each position. The lateral resolution afforded by the milliprobe is shown by the dashed lines of Figure 11, and the statistical fluctuations expected in the data are indicated approximately by the single uncertainty bar.

The data of Figure 11 support the recent finding that wear surfaces of certain implanted samples in general show little change except for a number of very fine scratches. This result is in contrast to the broad, U-shaped depression in the wear region typically observed in unimplanted samples. A measurement of the surface profile (Talysurf) over the region corresponding to the scar in Figure 11 shows a number of fine scratches in an otherwise undeformed surface (Fig. 11, upper half). The depression in the ^{15}N yield is consistent with a scratch having the same width as the largest scratch in the Talysurf profile, but the 35-μm displacement of the two signals is not presently understood. If the two signals are correlated, the milliprobe data indicate that approximately 75% of the original ^{15}N implant dose remains at a depth of 0.6 μm, or nearly ten times the original implant depth.

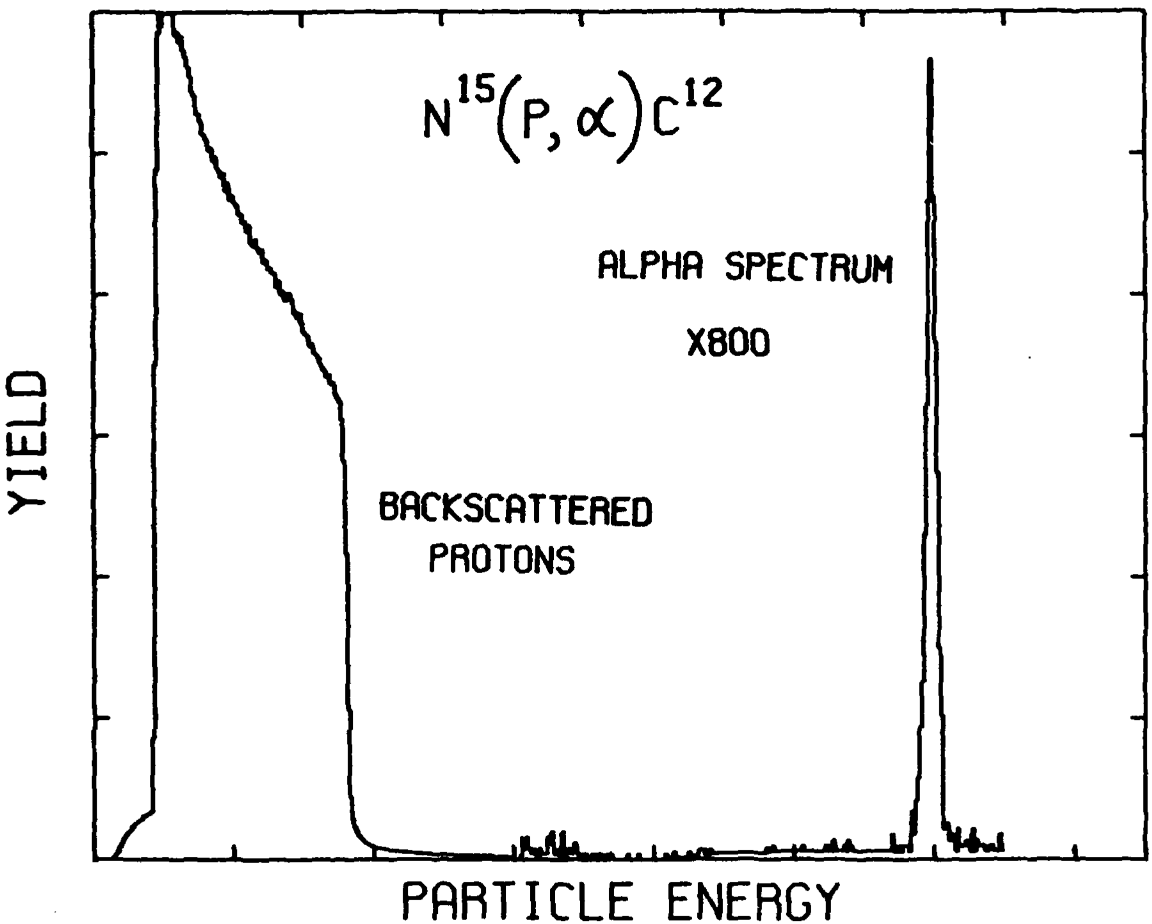

Fig. 10 - Spectrum produced by a 25-μm beam of 1.05-MeV protons incident on a ^{15}N-implanted stainless steel wear sample. The alpha particles produced by the $^{15}N\ (p\alpha)^{12}C$ reaction appear in the narrow peak at the high energy end of the spectrum. The area under the peak is proportional to the amount of ^{15}N present, and the width of the peak is an indication of its depth distribution.

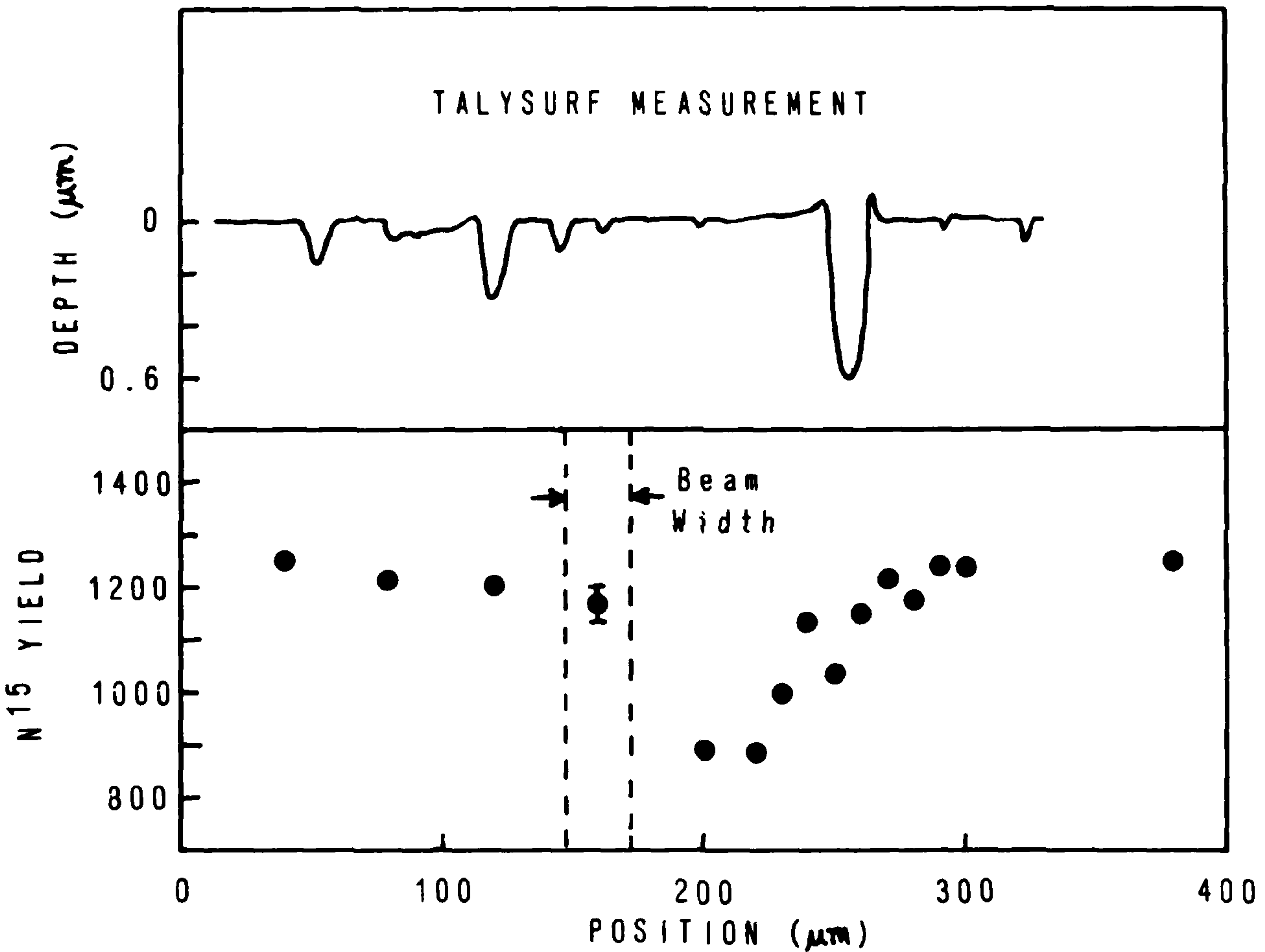

Fig. 11 - (Bottom) plot of ^{15}N yield versus position for a milliprobe scan across wear scar of ^{15}N-implanted stainless steel. (Top) talysurf surface profile measurement for the same region.

3.3. Changes Induced in N-Implanted Silicon by Laser Annealing

The implantation of nitrogen into silicon is being employed to change the infrared transmission characteristics of silicon. After implantation, annealing is necessary to obtain the maximum absorption at 10.6 μm. Laser annealing after ion implantation has recently been found to be a convenient and effective method of removing the damage produced by the implantation process and for making the atoms introduced by implantation electrically active in semiconductor devices. This technique is being applied to nitrogen-implanted silicon to determine its effectiveness in this situation. It has been found that when CO_2-laser radiation strikes a sample of nitrogen implanted silicon which is bevelled on one side, a pattern of light and dark fringes analogous to an optical thin-film interference pattern is produced on the surface [15]. Figure 12 shows a photograph of such fringes viewed through a microscope. The spacing between adjacent fringes is 83 μm. The surface shown in Figure 12 was bevelled at $1/2^{\circ}$ to the back surface so that the sample thickness changes uniformly from left to right. No fringes are observed in the upper half of the sample which was masked off during implantation. The annealing was done by a pulsed CO_2 laser (10.6 μm wavelength) with an energy density of 5 joules/cm^2. Because of the transparency of the silicon substrate at this wavelength the power absorbed in the silicon is probably insufficient to cause melting.

The cause of the fringes is ultimately the interference between the laser light wave transmitted through the front surface and that reflected from the rear surface of the sample. The largest amplitude of the electric field vector at the front surface of the sample, which should correspond to the greatest heating effect, is obtained when the sample is an integral number of half wavelengths in thickness. In this situation the portion of the incident wave reflected at the front surface has its smallest amplitude and the energy transmitted through the rear surface is largest.

The physical changes in the surface layer which cause the light and dark stripes are presently unknown. Several mechanisms have been suggested, including formation of an oxide layer after annealing, diffusion of the implanted nitrogen to the surface within the "hot" stripes, spallation of the surface in stripes due to thermal shock produced by the laser pulse, or regrowth of the surface in alternating stripes of amorphous and crystalline silicon.

Several samples exhibiting the fringing phenomenon were analyzed with the milliprobe in order to look for compositional differences between the light and dark fringes. The 83-μm width of the stripes would not allow analysis with the normal Van de Graaff beam-spot size. In order to minimize local heating effects due to the high power density of the focused beam, the beam was defocused to a rectangular image 35 μm wide by 150 μm long. Rutherford backscattering with 2-MeV He^+ ions revealed in most cases no significant differences in the nitrogen profile between adjacent stripes, and set an upper limit on oxide formation of 200 angstroms. One particular sample however displayed evidence of spallation on alternate stripes. This evidence is shown in Figure 13, which shows backscattering spectra from two adjacent stripes which appeared to be gold and silver colored, when viewed at the proper angle with a microscope. The spectrum obtained for the "silver" stripe agrees with expectations for an implant of 4×10^{17} nitrogen atoms per cm^2 at 75 keV. The "gold" stripe spectrum shows the nitrogen implant to be shifted toward the surface by about 1135 angstroms, with some nitrogen loss occurring at the surface as indicated by the reduced nitrogen peak intensity. These results are consistent with a spallation mechanism. More work however is necessary to understand the physical surface changes causing the fringing pattern.

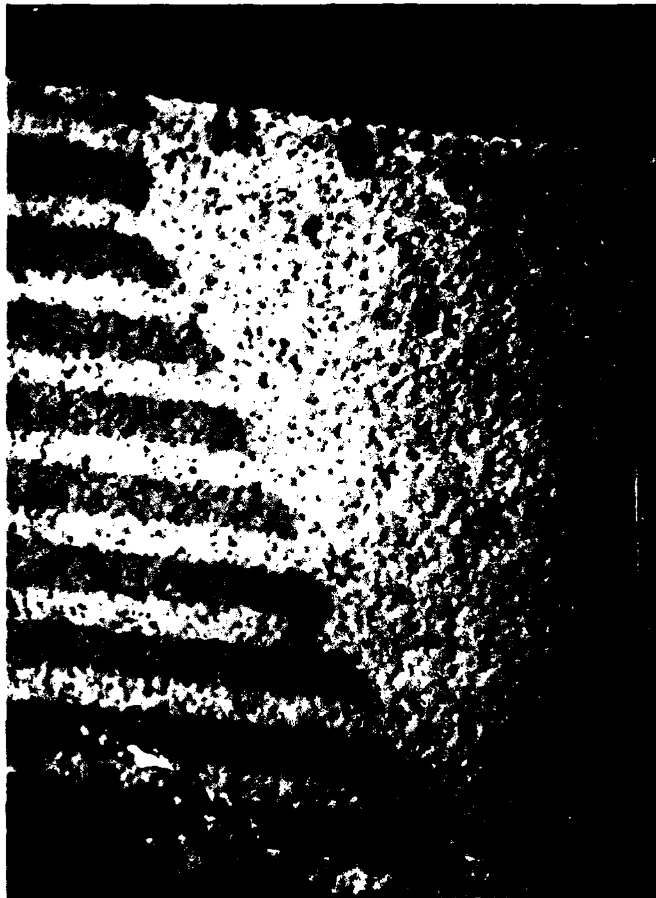

Fig. 12 - Optical micrograph (magnification of five) of silicon after implantation with 75-keV nitrogen ions and laser annealing treatment. One surface was polished at a 1/2° angle to the other surface. Note the uniform spacing of the stripes in the implanted region. The region free of stripes was unimplanted.

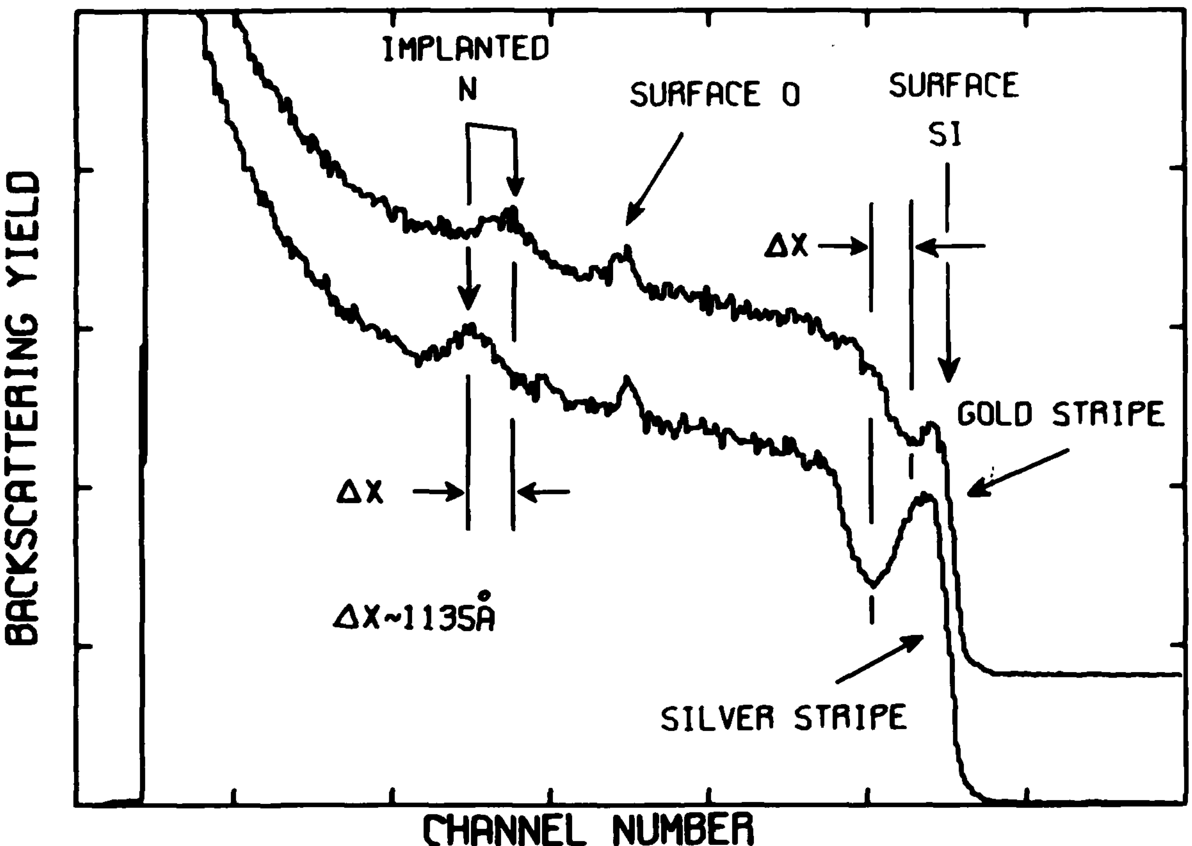

Fig. 13 - Milliprobe backscattering analysis for two adjacent stripes (83-μm spacing) on a sample of nitrogen-implanted and laser-annealed silicon. The "silver" stripe spectrum is as expected for 4×10^{17} nitrogen ions per cm^2 at 75 keV. The shift of the nitrogen by 1135 angstroms toward the surface of the "gold" stripe region can be deduced from changes in the position of both the nitrogen peak and the depression in the silicon yield due to its dilution by the implanted nitrogen. Evidence of surface oxygen is seen in both spectra. The nitrogen shift is evidence of spallation, probably from the thermal shock of the laser annealing treatment.

4. CONCLUSION

A variety of analytical applications for tightly focused ion beams is beginning to appear in the literature. For example, there are (i) studies of trace elements in inclusions in meteorites [4], which may provide information on their formation process, (ii) searches for superheavy elements in monazite grains [15], (iii) scanning of integrated circuit metallizations buried under silicon dioxide, performed nondestructively [9], and (iv) investigations of biological processes such as growth mechanisms in bones [3]. Ion microprobes have also been applied to metallurgical problems, and it is from this area that most applications of the NRL milliprobe are expected to come. It is anticipated that the good lateral resolution of the milliprobe, combined with the depth resolution, sensitivity, and specificity of ion beam analysis methods, will prove to be a powerful technique for attacking many materials problems and will make a significant contribution to the understanding of wear, corrosion, diffusion, and other processes.

Additional applications of the milliprobe may be found in the production of ion-implanted materials, where the tightly focused beam may be used to produce arbitrary patterns of dopant ions in the X-Y plane. Furthermore, by using ions with different ranges one may produce different patterns at various depths in the substrate material.

This work was carried out principally by R. D. Willis (during tenure as an NRC-NRL Postdoctoral Research Associate) and A. R. Knudson during the period from August 1977 to June 1979. C. A. Kennedy provided technical assistance and M. L. Herndon machined all of the fabricated items.

REFERENCES

[1] J. F. Ziegler, Ed., New Uses of Ion Accelerators (Plenum Press, New York, 1975).

[2] E. A. Wolicki, J. W. Butler, and P. A. Treado, Eds., Proceedings of the Third International Conference on Ion Beam Analysis, Nucl. Instr. and Meth. **149** (1978).

[3] R. E. Shroy, H. W. Kraner, and K. W. Jones, Nucl. Instr. and Meth. **157**, 163 (1978).

[4] F. Bosch, A. El Goresy, B. Martin, B. Povh, R. Nobiling, D. Schwalm, and K. Traxel, Nucl. Instr. and Meth. **149**, 665 (1978).

[5] W. M. Augustyniak, D. Betteridge, and W. L. Brown, Nucl. Instr. and Meth. **149**, 669 (1978).

[6] J. A. Cookson, A. T. G. Ferguson, and F. D. Pilling, J. Radioanal. Chem. **12**, 39 (1971).

[7] R. Nobiling, Y. Civelekoglu, B. Povh, D. Schwalm, and K. Traxel, Nucl. Instr. and Meth. **130**, 325 (1975).

[8] P. Horowitz, M. Aronson, L. Grodzins, W. Ladd, J. Ryan, G. Merriam, and C. Lechene, Science **194**, 1162 (1976).

[9] P. Bayerl and P. Eichinger, Nucl. Instr. and Meth. **149**, 663 (1978).

[10] H. R. Wilde, M. Roth, C. D. Uhlhorn, and B. Gonsior, Nucl. Instr. and Meth. **149**, 675 (1978).

[11] D. Brune, U. Lindh, and J. Lorenzen, Nucl. Inst. and Meth. **142**, 51 (1977).

[12] Trademark, E. I. du Pont de Nemours and Co., Inc., Wilmington, Delaware.

[13] Trademark, High Voltage Engineering Corporation, Burlington, Massachusetts.

[14] J. K. Hirvonen, J. Vac. Sci. Technol. **15**, 1662 (1978).

[15] T. A. Kennedy, G. E. Matthews, G. K. Hubler, private communication.

[16] F. Bosch, A. El Goresy, W. Kratschmer, B. Martin, R. Nobiling, B. Povh, D. Schwalm, and K. Traxel, Z. Physik **A280**, 39 (1977); Phys. Rev. Lett. **37**, 1515 (1976).

END

DATE
FILMED
8-80

DTIC